A 15-Year Climatology of Warm Conveyor Belts

SABINE ECKHARDT AND ANDREAS STOHL*

Department of Ecology, Technical University of Munich, Freising-Weihenstephan, Germany

HEINI WERNLI

Institute for Atmospheric and Climate Science, ETH Zürich, Zürich, Switzerland

PAUL JAMES, CAROLINE FORSTER, AND NICOLE SPICHTINGER

Department of Ecology, Technical University of Munich, Freising-Weihenstephan, Germany

(Manuscript received 2 January 2003, in final form 16 June 2003)

ABSTRACT

This study presents the first climatology of so-called warm conveyor belts (WCBs), strongly ascending moist airstreams in extratropical cyclones that, on the time scale of 2 days, rise from the boundary layer to the upper troposphere. The climatology was constructed by using 15 yr (1979–93) of reanalysis data and calculating 355 million trajectories starting daily from a $1° \times 1°$ global grid at 500 m above ground level (AGL). WCBs were defined as those trajectories that, during a period of 2 days, traveled northeastward and ascended by at least 60% of the zonally and climatologically averaged tropopause height. The mean specific humidity at WCB starting points in different regions varies from 7 to 12 g kg^{-1}. This moisture is almost entirely precipitated out, leading to an increase of potential temperature of 15–22 K along a WCB trajectory. Over the course of 3 days, a WCB trajectory produces, on average, about four (six) times as much precipitation as a global (extratropical) average trajectory starting from 500 m AGL. WCB starting points are most frequently located between approximately 25° and 45°N and between about 20° and 45°S. In the Northern Hemisphere (NH), there are two distinct frequency maxima east of North America and east of Asia, whereas there is much less zonal variability in the Southern Hemisphere (SH). In the NH, WCBs are almost an order of magnitude more frequent in January than in July, whereas in the SH the seasonal variation is much weaker. In order to study the relationship between WCBs and cyclones, an independent cyclone climatology was used. Most of the WCBs were found in the vicinity of a cyclone center, whereas the reverse comparison revealed that cyclones are normally accompanied by a strong WCB only in the NH winter. In the SH, this is not the case throughout the year. Particularly around Antarctica, where cyclones are globally most frequent, practically no strong WCBs are found. These cyclones are less influenced by diabatic processes and, thus, they are associated with fewer high clouds and less precipitation than cyclones in other regions. In winter, there is a highly significant correlation between the North Atlantic Oscillation (NAO) and the WCB distribution in the North Atlantic: In months with a high NAO index, WCBs are about 12% more frequent and their outflow occurs about 10° latitude farther north and 20° longitude farther east than in months with a low NAO index. The differences in the WCB inflow regions are relatively small between the two NAO phases. During high phases of the Southern Oscillation, WCBs occur more (less) frequent around Australia (in the South Atlantic).

1. Introduction

The global atmospheric circulation is characterized by the poleward transport of energy in terms of both sensible and latent heat (Peixoto and Oort 1992). In the Tropics, where the Coriolis force is small, the energy transport is accomplished via zonally almost symmetric convective overturning, that is, the Hadley cell. Outside the Tropics, a westerly thermal wind is established between the warmer low latitudes and the colder high latitudes. Such a jetlike flow is baroclinically unstable, resulting in baroclinic waves transporting the energy poleward. Essential features of these baroclinic waves are the embedded cyclones and anticyclones that account for most of the atmospheric variability in the midlatitudes on synoptic time scales (Trenberth 1991). The fronts associated with the cyclones are particularly noteworthy, as they produce a major fraction of both the upward and poleward moisture transport and the pre-

* Current affiliation: CIRES, University of Colorado/NOAA Aeronomy Laboratory, Boulder, Colorado.

Corresponding author address: Sabine Eckhardt, Department of Ecology, Technical University of Munich, Am Hochanger 13, D-85354 Freising-Weihenstephan, Germany.
E-mail: eckhardt@forst.tu-muenchen.de

cipitation in the midlatitudes (Stewart et al. 1998). Baroclinic waves are also important for the transport of chemical trace constituents in the atmosphere (Wang and Shallcross 2000). Furthermore, extratropical cyclones vent the atmospheric boundary layer (ABL) (Cotton et al. 1995) and, thus, are crucial for cleansing the ABL from air pollution and aerosols.

Since cyclones are such an important component of the climate system, it is not surprising that much effort has been put into the characterization of their geographical distribution. Because of the location of landmasses, it is far from zonal uniformity, in particular in the Northern Hemisphere (NH), where cyclones are concentrated over the Atlantic and Pacific Oceans (Gulev et al. 2001; Sickmöller et al. 2000; Hoskins and Hodges 2002). In the Southern Hemisphere (SH), the cyclone distribution shows less zonal variability (Sinclair 1994; Simmonds and Keay 2000a,b).

Different methods exist for constructing cyclone climatologies, most of which diagnose cyclone centers (e.g., by identifying pressure or geopotential height minima at various levels in the troposphere, or relative vorticity maxima in the lower troposphere) and track them over the cyclone's life cycle [see Hoskins and Hodges (2002), for a comparison of some techniques]. However, technical problems exist with these methods (e.g., unrealistic reduction of pressure to sea level over topography, ambiguous tracking algorithms). Thus, it is not surprising that existing cyclone climatologies are in modest agreement with each other, particularly in the SH. Many of the identified structures may be heat lows or lee troughs that have limited vertical extent and are not associated with deep clouds or significant amounts of precipitation (Sinclair 1994). Furthermore, there is no simple relation between, say, the depth of a surface pressure minimum and important properties of the corresponding cyclone (e.g., its transport of heat, water vapor, and trace gases, or cloud and rain formation). For instance, Martin (1998) and Iskenderian (1988) discussed the case of a very modest surface cyclone, which produced extremely heavy snowfall over North America. This limits the significance of existing cyclone climatologies. An attractive alternative to these climatologies therefore would be to diagnose, instead, directly those airstreams that produce the largest portion of a cyclone's precipitation and cause most of its meridional heat transport.

The study of airflows associated with extratropical cyclones has a long history and goes back to the development of the Bergen school cyclone model (e.g., Bjerknes 1910). Later, the quasi-Lagrangian conveyor belt model was developed by Harrold (1973), Browning et al. (1973), and Carlson (1980) (see also Browning 1990, 1999; Carlson 1998). This model describes three airstreams in a coordinate system moving with the cyclone. They are typically of the order of 1 km in depth and a few hundred kilometers across. The dry intrusion (DI) descends behind the cold front from the upper troposphere and/or lower stratosphere to the lower troposphere. The cold conveyor belt (CCB) splits into two branches; an anticyclonic branch, which ascends ahead of the surface warm front from the ABL into the middle troposphere and a cyclonic branch, which remains in the lower troposphere (Schultz 2001). The warm conveyor belt (WCB), experiencing the strongest vertical motion of the three airstreams, ascends slantwise ahead of the surface cold front from the ABL all the way into the upper troposphere, where it may override the CCB. The WCB originates in the cyclone's warm sector and is responsible for most of the cyclone's meridional energy transport, in terms of both latent and sensible heat. In infrared satellite images, WCBs are clearly visible as bright frontal cloud bands, which forecasters associate with maturing cyclones. WCBs furthermore appear as so-called atmospheric rivers in global maps of the vertically integrated water vapor flux, with a water flow comparable to that of the Amazon (Newell et al. 1992).

From a dynamical standpoint, WCBs are important for the evolution of the cyclone they pertain to, for the potential formation of downstream upper-level anticyclones, and for the rapid transport of ABL air into the upper troposphere and lowermost stratosphere (Wernli and Bourqui 2002). WCBs constitute a Lagrangian manifestation of the impact of latent heat release on cyclone development. The general picture is that condensational heating leads to the production of positive potential vorticity (PV) anomalies in the lower/middle troposphere (e.g., Stoelinga 1996; Wernli and Davies 1997) and finally to an enhancement of cyclone development that is otherwise determined by dry dynamics (e.g., Kuo et al. 1991; Davis et al. 1993). WCBs also develop in model simulations with dry dynamics only, but these are less strong than when also moist processes are accounted for. This suggests that the occurrence of a prominent WCB in the vicinity of an extratropical cyclone hints at a rapid storm development, potentially also leading to explosive genesis of so-called bombs (Sanders and Gyakum 1980; Zhu and Newell 1994). It will therefore be of interest to verify whether WCBs are most frequent in regions of preferred rapid cyclogenesis. Also of relevance are the upper-level effects induced by WCBs. After the ascent phase, WCBs arrive in the upper troposphere with low tropospheric PV values (typically $<$0.6 PV units; Wernli 1997; Pomroy and Thorpe 2000). At the level of the WCB outflow, these values can correspond to significant negative PV anomalies in the upper troposphere. Low-PV air masses in the upper troposphere are important, for instance, for maintaining blocking (e.g., Mullen 1987), and C. B. Schwierz et al. (2003, unpublished manuscript) identified the significant role of PV modification in WCBs for the sustenance of North Atlantic blocking. Massacand et al. (2001) presented a case where the upper-level anticyclonic flow, enhanced by the outflow of a WCB, contributed to the downstream formation of a PV streamer. Some of the

WCB outflow can enter the stratosphere during the days after the ascent (Stohl 2001). The physical processes leading to the associated PV increase are not yet fully understood, but one hypothesis is that radiation induces significant PV changes near the maximum vertical moisture gradient (Zierl and Wirth 1997).

Large differences also exist between the chemical characteristics of the airstreams in a cyclone (Bethan et al. 1998), leading to an extension of the conceptual conveyor belt model to include also the airstream's chemical composition (Cooper et al. 2001, 2002). Recently, WCBs have been found to be important for the long-range transport of air pollution, for instance, intercontinental transport of sulfur (Arnold et al. 1997), ozone (Stohl and Trickl 1999), and ozone precursors (Stohl et al. 2003). WCBs transport these substances to the tropopause region, thus enhancing possible effects on the radiative forcing of the earth–atmosphere system. They also influence the formation and properties of cirrus clouds through the upward transport of both moisture and ice nuclei (Rogers et al. 1998), may trigger ion-induced nucleation of aerosols (Stohl et al. 2003), and favor the development of contrails (Kästner et al. 1999). Thus, WCBs have tremendous effects not only on the atmospheric energy and moisture budgets, but on the climate system as a whole. Despite their great importance, no attempt has been made yet to determine their global geographical distribution over longer time periods. In this paper, we present a first 15-yr climatology of WCBs using meteorological reanalysis data.

One method to diagnose WCBs in global meteorological datasets uses trajectories, which emphasizes their Lagrangian nature. In case studies, Wernli and Davies (1997) and Wernli (1997) have shown that WCBs are associated with coherent ensembles of trajectories with characteristic properties (e.g., strong ascent, strong decrease in water vapor and corresponding increase in potential temperature, poleward and eastward motion) that can be used to diagnose WCBs in a global trajectory dataset. Stohl (2001) has used this method to establish a first 1-yr ''climatology'' of WCBs and other airstreams in the NH, which revealed two maxima in the frequency of WCB inflow, located south of the entrance to the two storm tracks.

In this paper we extend Stohl's (2001) study to both hemispheres and a 15-yr period, and develop a detailed characterization of WCBs. In section 2 we explain our WCB identification procedure and demonstrate it in a case study. In section 3 we discuss the main properties of WCBs and present their 15-yr climatology, which then is compared with a cyclone climatology in section 4. In section 5 we examine the relationship between WCBs and precipitation. The interannual variability of WCB occurrence, and its relationship to important measures of climate variability, is studied in section 6. Finally, conclusions are drawn in section 7.

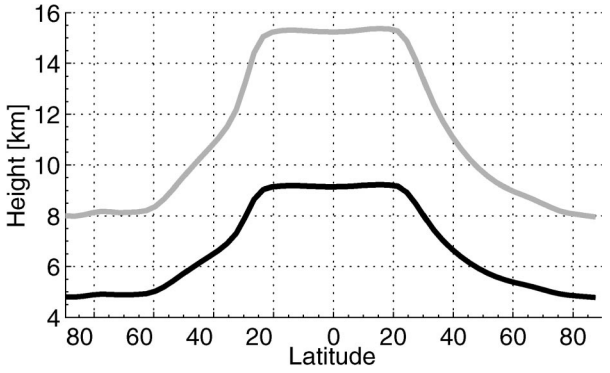

FIG. 1. Zonally averaged tropopause height (gray line) and 60% of the zonally averaged tropopause height (black line) as a function of latitude.

2. Methods and an illustrating case study

a. Trajectory calculations

Three-dimensional trajectory calculations were carried out with the Lagrangian model FLEXTRA (Stohl et al. 1995; Stohl and Seibert 1998), which is used with wind fields from the European Centre for Medium-Range Weather Forecasts (ECMWF). Details on FLEXTRA can be obtained online (at http://www.forst.tu-muenchen.de/EXT/LST/METEO/stohl/flextra.html). An intercomparison of FLEXTRA with other trajectory models can be found in Stohl et al. (2001). For this study we have used the ECMWF 15-yr re-analysis dataset (ERA-15), which was produced with a T106 spectral model (Gibson et al. 1999) and covers the years from 1979 to 1993. We retrieved these data from the ECMWF archives with a resolution of $1° \times 1°$, 31 levels, and every 6 h. Six-day forward trajectories were started at 500 m AGL on a global grid of $1° \times 1°$ resolution at 1200 UTC every day, which gives a total number of 355 million trajectories. The model output consisted of the trajectory positions, and values of PV, potential temperature Θ, specific humidity q, and pressure along the trajectories every 24 h.

b. WCB selection criteria

As seen in a case study presented below and in Wernli and Davies (1997), the trajectories associated with a WCB are characterized by rapid ascent and transport first poleward, and then eastward within about two days. We used these features to identify WCBs automatically in the 15-yr global dataset. A trajectory was classified as a WCB trajectory if, during the first 2 days, it traveled more than 10° longitude to the east and more than 5° latitude to the north, and ascended by more than 60% of the zonally and climatologically averaged tropopause height at the trajectory's latitudinal position after 2 days. This accounts for the fact that WCBs start in the ABL and rise within about two days to the upper troposphere.

Zonal mean tropopause heights were calculated from

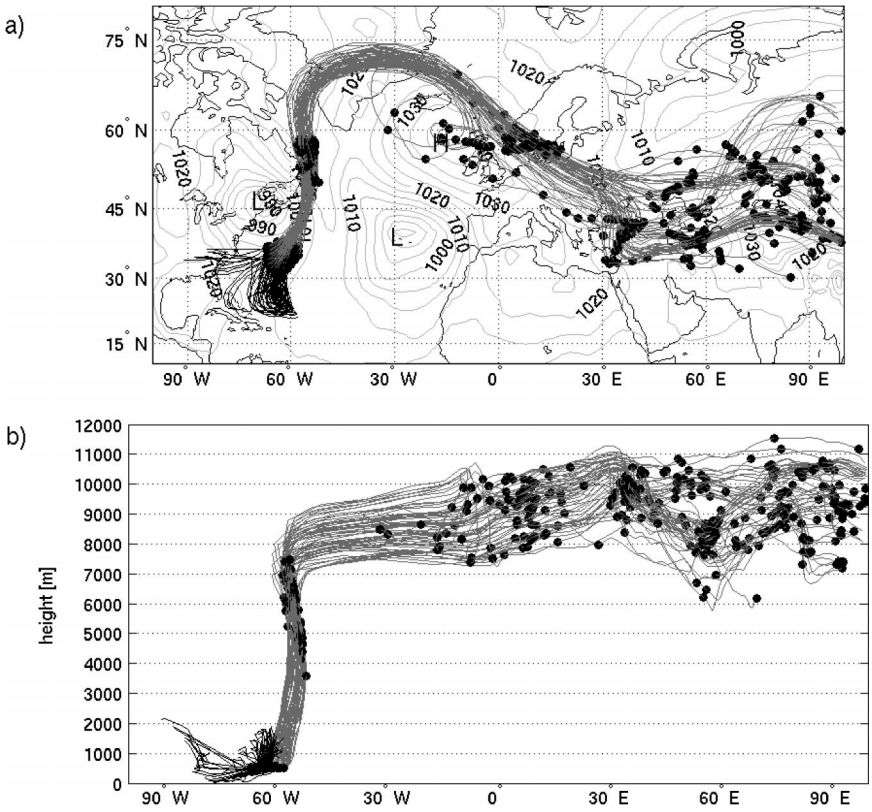

FIG. 2. Six-day trajectories starting 1200 UTC 23 Jan 1987, of which the first 2 days were identified as a WCB. (a) The forward trajectories (gray) and 3-day backward trajectories (black) from the starting locations of the forward trajectories. Positions along the forward trajectories are marked every 24 h. Sea level pressure (light gray) contour lines are drawn every 10 hPa for the trajectory starting time (1200 UTC 23 Jan 1987). For clarity, only those WCB trajectories associated with the cyclone over the eastern seaboard of North America are drawn. (b) Vertical projection of the trajectories shown in (a).

the ECMWF data and are shown as a function of latitude in Fig. 1. A thermal tropopause criterion (WMO 1957) was used in the Tropics (20°S to 20°N) and a dynamical one (2 PV units) poleward of 30° (Hoskins et al. 1985), respectively. In the region between $\pm 20°$ and $\pm 30°$ we interpolated between the thermal and the dynamical tropopause linearly. In the midlatitudes the threshold height for WCB trajectories after 2 days varies from about 8 (30°) to 5 km (>60°).

Any criterion used for an automatic classification of WCBs is necessarily subjective. We designed our criteria to be conservative in a sense that only the cores of reasonably strong WCBs shall be identified, whereas trajectories close to the airstream's boundaries—where rapid dispersion occurs (Cohen and Kreitzberg 1997)—and also weak WCBs shall not be identified. However, while the absolute number of WCB trajectories is highly sensitive to variations of our criteria, the identified spatial patterns of WCB frequency are very robust. Stohl (2001) used a constant ascent criterion of 8000 m instead of the one used here, which depends on the latitude, causing a tendency to underestimate the frequency of WCBs at high latitudes. However, even with Stohl's (2001) criteria the identified spatial patterns were quite similar. The criteria requiring a northward and eastward motion are effective in preventing airstreams in the Tropics from being misclassified as WCBs and were used already by Stohl (2001). The algorithm may occasionally miss cyclonically turning WCBs, in particular ''trowal''-type airstreams, which can turn westward (Martin 1998), at least in a quasi-Lagrangian coordinate system moving with the cyclone. But over the time period of 2 days and in an absolute coordinate system even those airstreams often travel sufficiently far to the east in order to be correctly classified as WCBs. In fact, imposing the eastward-moving criterion leads to a global reduction of the WCB mass fluxes of only 20%, compared to a doubling for a reduction of the ascent criterion by 10%. However, without this criterion, sometimes tropical airstreams (e.g., in hurricanes) would have been misclassifed as WCBs.

c. A case study example

To illustrate our methodology, we present a typical example of a WCB occurring in the North Atlantic on

23 January 1987. Note that, for better visualization, we have recalculated this case with a more frequent (every 2 h) position output along the trajectories than is available in the 15-yr climatology, but the 24-hr positions used for the classification are also marked. Figure 2 shows the 60 trajectories (gray lines) that fulfilled the WCB criterion. They started in the western Atlantic between 30° and 40°N and reached the east coast of Newfoundland after the first day. The northward movement was accompanied by rapid ascent to 5–7 km. One day later, after passing southern Greenland, the trajectories were located between 7 and 11 km over the eastern Atlantic and Scandinavia. During these first 2 days, the trajectories were organized as a coherent bundle and jointly traveled in a wavelike manner, much the same as in the case study of Wernli and Davies (1997). On the following days they moved farther to the east with relatively little change in altitude and with less speed than on the second day. Note also the loss of coherency of the trajectory ensemble after 2 days. This is typical (see also Wernli 1997, Fig. 6), confirming the 2-day period used to identify WCBs in our climatology.

At the beginning, the trajectory ensemble was located to the southeast of a cyclone's center (Fig. 2), in its warm sector. During the next day, the cyclone moved to Labrador, while the WCB moved rapidly to the north. Thus, after 1 day the WCB was located to the east of the cyclone's center, within a distance of 1000 km. During the second day the cyclone weakened west of Greenland and finally died over the Baffin islands. The trajectories turned anticyclonically, left the cyclone and were located over northwestern Europe at the end of the second day. Both the shape and the location of these WCB trajectories relative to the cyclone's center during the course of the 2 days of ascent look very similar to the more schematic depictions of airstreams in a cyclone (e.g., Carlson 1980) and the satellite cloud patterns (not shown). This provides further evidence that our algorithm indeed identified a WCB.

To explore where the air entering the WCB came from, we calculated 3-day backward trajectories from the starting points of our forward trajectories (black lines in Fig. 2). This low-level inflow was much slower than the transport in the WCB itself and the subsequent motion in the upper troposphere. Due to the confluence in the cyclone's warm sector, WCB trajectories rapidly separate backward in time. Therefore, a WCB's source region can be quite large (see also Wernli 1997, Fig. 6). WCBs, thus, also have considerable transporting potential for polluted air to the upper troposphere.

The inflow of air into a WCB occurs in the lowermost troposphere. If we assume that our trajectories, which were started at 500 m AGL, are representative for this inflow, and furthermore that the inflow depth is 1000 m, we can calculate the mass of air and moisture transported with the WCB. Note that if trajectories were started from several levels in the lower troposphere (which was not possible for computational reasons), we could have determined the mass fluxes explicitly. However, scaling with a constant inflow depth serves our purpose of converting trajectory numbers into mass fluxes, which can be reported and compared more conveniently. If we apply the above procedure to our case study, we find that this WCB transported 7700×10^6 kg s^{-1} and 98×10^6 kg s^{-1} of air and water, respectively. This moisture flux is about 59% of the flow in the Amazon river [165×10^6 kg s^{-1} according to Newell et al. (1992)]. As we have only identified the WCB's core, its total moisture flux, in fact, has exceeded that of the Amazon river (see below).

Knowing the mass of a WCB air parcel, we can also calculate the amount of precipitation it causes, using the decrease of q along its trajectory. The assumptions we use for this calculation are, first, that a WCB air parcel does not take up significant amounts of moisture from the surface or from evaporating hydrometeors falling into it. This assumption is largely valid, because of the strong ascent, and thus rapid transport away from the surface of a WCB trajectory. The second assumption is that the decrease in q along a trajectory is fully realized as precipitation. Certainly this assumption is violated to some extent as not all hydrometeors formed upon ascent will precipitate out, and some of them may evaporate in the drier air beneath the WCB. Despite these limitations our precipitation estimates are in good agreement with precipitation fields from other sources (see section 5). For our case study WCB, we find that almost 100% of the moisture inflow is precipitated out, yielding a total precipitation amount of 8.4×10^{12} kg. If we assume that the decrease of q between two subsequent trajectory points has precipitated out in the middle of the two positions, we can also produce precipitation maps. In our example, the precipitation fell over an area of roughly 7 million km^2, yielding an average precipitation of 1.2 mm in this region.

Our reported mass and moisture fluxes are valid only for the WCB's core, which we capture with our strong ascent criteria. In an attempt to quantify how much mass and moisture may be uplifted by a WCB outside its core (but still close to it), we repeated our calculations for this case study with modified criteria. We counted all trajectories that started in the southern part of the cyclone around the WCB core trajectories' starting locations (in a region from 85°W to 50°W and 25°N to 50°N) and that crossed the 850-hPa level. This increased the mass and moisture fluxes by factors of 9 and 5, respectively, and the amount of precipitation by a factor of 4, compared to when the WCB's core alone is considered. Unfortunately, this procedure cannot be applied automatically for our 15-yr climatology, because the region where trajectories should be considered as belonging to the WCB, varies with the size and shape of a cyclone and requires careful manual adjustment. However, the factors found here may serve as a proxy to upscale our results found for the WCB cores.

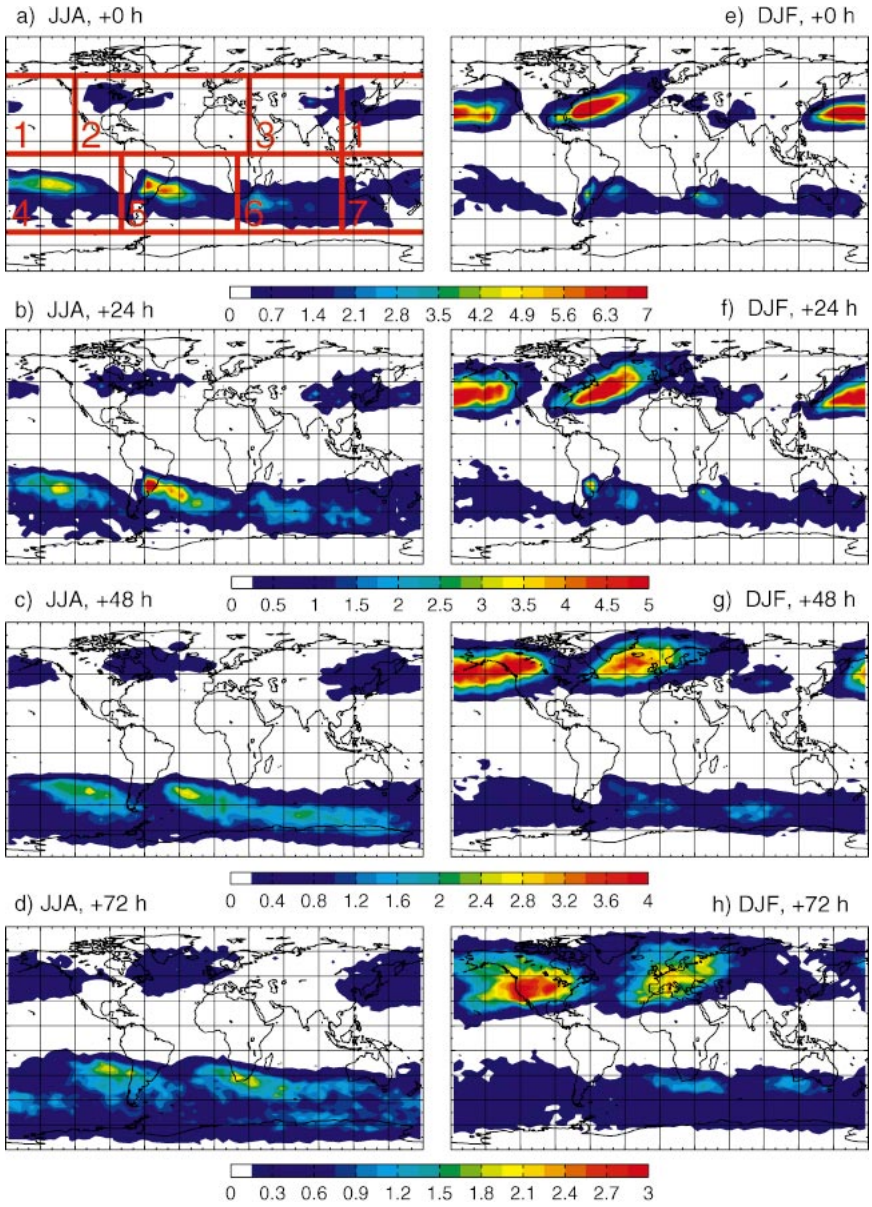

FIG. 3. Seasonal mean spatial distribution of (a), (e) WCB starting points and WCB trajectory positions after (b) and (f) 24, (c) and (g) 48, (d) and (h) 72 h for (a)–(d) JJA and (e)–(g) DJF. Depicted is the fraction (in percent) of all trajectories that fulfill the WCB criteria, averaged over 15 yr. For clarity, different color scales were used for the different days. The red rectangles in (a) numbered from 1 to 7 show the boxes used for further analyses.

3. Spatial distribution and mean properties of WCBs

a. The geographical distribution of WCBs

Figure 3 shows the spatial distribution of WCB starting points (Figs. 3a,e) and WCB positions after 24 h (Figs. 3b,f), 48 h (Figs. 3c,g) and 72 h (Figs. 3d,h), respectively, averaged over all 15 yr for June–August (JJA) (Figs. 3a–d) and DJF (Figs. 3e–h). WCBs occur more frequently during winter than during summer. This seasonal cycle is particularly strong over the North Atlantic and North Pacific (with about eight times more WCBs during winter than during summer) and weaker on the SH. The highest WCB starting point frequencies are found between approximately 25° and 45°N and between about 20° and 45°S. Maximum values amount to about 10% in winter, meaning that on 10% of all days the trajectories released at this point at 500 m AGL fulfill the WCB criteria. In both hemispheres, we find that in summer WCB trajectories start at higher latitudes than in winter. In the NH, there are two distinct maxima east of North America and east of Asia, whereas very

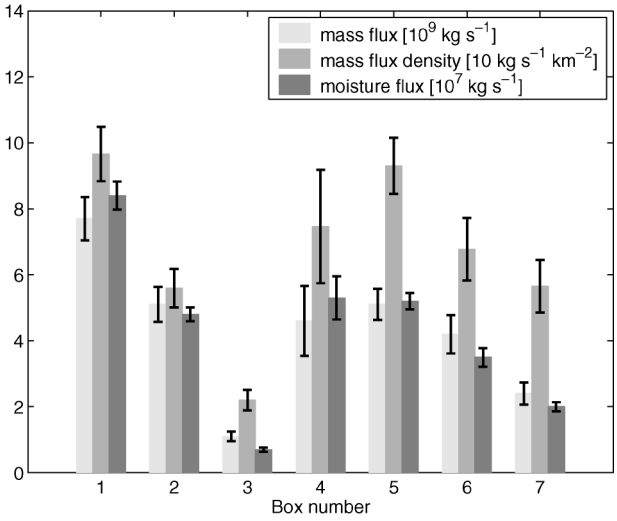

FIG. 4. Fifteen-year annual mean WCB mass fluxes, mass flux densities, and moisture fluxes for the seven boxes shown in Fig. 3. Standard deviations have been calculated from the values in individual years and are shown by the whiskers.

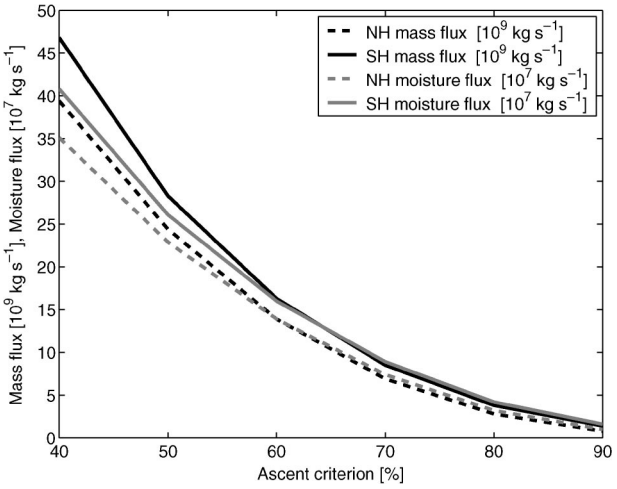

FIG. 5. Sensitivity of the 15-yr mean total WCB mass fluxes (10^9 kg s^{-1}) and moisture fluxes (10^7 kg s^{-1}) in the NH and SH, respectively, to variations of the ascent criterion (given in % of the tropopause height).

few WCBs originate from Eurasia and western North America. These patterns are consistent with those identified by Stohl (2001) for a 1-yr period. In the SH, there is much less zonal variability than in the NH. Two maxima are located east of South Africa and east of South America but, except for a small region over the cold surface waters west of South America, WCBs originate quite frequently from all longitudes. The maximum over South America is exceptional, because it also covers large continental areas. As will be shown later, cyclogenesis in the lee of the Andes mountain range as well as the formation of a heat low over land are important reasons for this maximum over land.

WCB trajectories travel poleward and eastward during the first 2 days (Figs. 3b,c,f,g), but turn equatorward thereafter (Figs. 3d,h). As in the case study (Fig. 2), this is due to the WCB outflow typically turning anticyclonically. The transport is fastest on day 2, when the WCB trajectories approach the jet stream in the upper troposphere. In both hemispheres, the eastward propagation is much slower during summer than during winter (compare, e.g., Figs. 3d and 3h), in agreement with the strength of the meridional thermal contrast and the associated thermal wind. Remarkably, the climatologically averaged WCB inflow (i.e., trajectory points at day 0) is much more focused on specific regions than the outflow (i.e., trajectory points after 2 days). The inflow regions are strongly influenced by surface forcings, particularly by sea surface temperatures above the zonal average.

After traveling 4 (in DJF) to 6 (in JJA) days (not shown), the North Pacific WCB trajectories are located most frequently over California, and the North Atlantic WCB trajectories over the Mediterranean, which indicates that WCBs can transport pollution from one continent to the other on timescales of a few days only, in agreement with tracer studies (Stohl et al. 2002).

b. WCB mass fluxes and mean properties

As the WCB distribution is quite heterogeneous, we study their properties in seven different boxes [see Fig. 3; the boxes on the NH are named N Pacific (1), N Atlantic (2), Asia (3), and on the SH: S Pacific (4), S Atlantic (5), Indian Ocean (6), and Australia (7)]. Substantial differences are found between the climatologically averaged WCB mass fluxes in these boxes (Fig. 4), with the smallest flux in Asia being almost one order of magnitude smaller than the largest flux in the North Pacific. Even if we account that the box sizes are somewhat different, we still find differences of more than a factor of 4 between the mass flux densities in the NH boxes, whereas the differences between the SH boxes are less than a factor of two. If we compare these mass fluxes with the mass flux in our example in section 2 (7.7×10^9 kg s^{-1}), we see that on average, only about one WCB of such strength is present in a box at a time. The greatest interannual variation (standard deviation of annual mass fluxes in Fig. 4) is found in the South Pacific, the North Pacific, and the Indian Ocean. We come back to this in section 6.

Figure 5 shows 15-yr mean WCB mass fluxes for the two hemispheres, obtained for several variations of our standard (i.e., 60% of the tropopause height) ascent criterion. The mass fluxes are highly sensitive to changes of the ascent criterion, decreasing by more than an order of magnitude for doubling the required ascent from 40% to 80%. However, neither the geographical position nor the relative strengths of the frequency maxima change significantly when changing the ascent criterion (not shown). Depending on the criterion used, the mass flux-

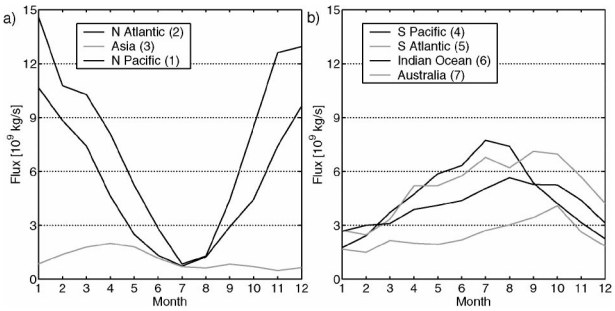

FIG. 6. Annual variation of the monthly mean WCB mass fluxes (10^9 kg s^{-1}) for the seven boxes shown in Fig. 3.

es are 20%–60% higher in the SH than in the NH, which is due to the smaller continental area, the larger evaporation, and a higher summertime WCB frequency in the SH. There is also a lower sensitivity to changes in the ascent criterion in the SH compared to the NH. Especially strong WCB ascent, thus, occurs more often in the SH than in the NH.

Figure 6 shows the seasonal variation of WCB mass fluxes for the seven boxes. In both hemispheres, there is a large seasonal variation in the frequency of WCBs, with a winter maximum and a summer minimum. The seasonal cycle is clearly larger in the NH than in the SH. It is largest in the North Pacific, where WCB mass fluxes are about one order of magnitude greater in January than in July. The South Atlantic box, which also covers land areas in South America, is exceptional, because there the highest mass fluxes occur in spring (September and October) rather than in winter. In monthly maps of the WCB distribution (not shown) it is clearly seen that the spring maximum in the South Atlantic is due to an intensification of WCB activity over land as compared to the winter, because of the stronger land surface heating. Such a spring maximum occurs also over the Asian continent.

What is the global relevance of the WCB mass fluxes compared to the mass fluxes due to other processes? For the purpose of answering this question we compare WCB mass fluxes with those produced by other cloud systems as reported in a review article by Cotton et al. (1995), who considered thunderstorms (scales up to about 30 km), mesoscale convective systems (scales up to about 200 km plus squall lines with length scales up to more than 1000 km), and mesoscale convective complexes (systems that produce a stratiform anvil cloud over 100 000 km^2), tropical cyclones, and extratropical cyclones (these include WCBs). The values given in Cotton et al. (1995) are for the transport of ABL air through the 900-hPa surface, whereas ours are for the transport of ABL air to above 40%, 60%, and 80% of the tropopause height (Table 1), respectively, within 48 h, which makes the comparison difficult. Unfortunately, to our knowledge, no appropriate global figures of ABL mass fluxes through higher levels in the troposphere are available for comparison. Nevertheless, the comparison

TABLE 1. Comparison of global mass fluxes (10^9 kg s^{-1}) and global annual precipitation (10^{15} kg) produced by WCB trajectories identified with ascent criteria of 40%, 60%, and 80% of the tropopause height, respectively, with the upward mass flux of boundary layer air across 900 hPa, and precipitation for several different types of cloud systems, taken from the review by Cotton et al. (1995).

Cloud system	Global mass flux	Annual precipitation
WCB cores 40	86	26
WCB cores 60	30	10
WCB cores 80	6.6	2.6
Extratropical cyclones	750	130
Tropical cyclones	24	12
Ordinary thunderstorms	211	56
Mesoscale convective systems	580	283
Mesoscale convective complexes	0.7	3.6

shown in Table 1 is useful. With our standard 60% ascent criterion, WCB mass fluxes into the upper troposphere are about 4% of the total mass flux across 900 hPa in cyclones. If we apply the factor of 9 found in the case study in section 2 to upscale our WCB mass fluxes for the crossing of the 850-hPa level [which is still a stronger criterion than the 900 hPa used by Cotton et al. (1995)], WCBs would account for more than a third of the upward flux in cyclones. Our WCB core mass fluxes are larger than those in tropical cyclones and mesoscale convective complexes, but are about an order of magnitude smaller than those in mesoscale convective systems and thunderstorms. After upscaling, WCB mass fluxes would be comparable to those in mesoscale convective systems and thunderstorms, though. Since the seasonal cycle of WCBs is opposite to that of the convective systems, WCB mass fluxes dominate over these in winter.

In the following we characterize WCBs by their average ascent, decrease in q and increase in Θ, and the fraction of air transported into the stratosphere. In all boxes the 15-yr mean pressure at the WCB starting point (at 500 m AGL) is around 940 hPa (Table 2), except for Asia, due to its topography. Pressure decreases by approximately 550 hPa during the first 2 days, and increases by about 20 hPa day^{-1} thereafter. The average ascent during the first 48 h is similar for all boxes, whereas the subsequent descent shows considerable differences. It is greatest in the South Atlantic (32 hPa day^{-1}), and generally faster in the SH than in the NH.

WCBs are associated with a strong decrease in q. The climate-mean q at their starting position is between 7

TABLE 2. Fifteen-year climate-mean pressure (hPa) at days 0–3 along the WCB trajectories, for the seven boxes shown in Fig. 3.

Box number	1	2	3	4	5	6	7
After 0 h	945.9	927.9	845.6	951.5	931.9	941.9	940.9
After 24 h	690.1	680.6	556.1	693.4	670.5	707.2	698.7
After 48 h	366.5	382.9	332.5	371.1	361.4	395.4	390.8
After 72 h	386.6	399.2	361.2	386.9	393.0	425.9	410.1

TABLE 3. Fifteen-year climate-mean specific humidity q (g kg^{-1}) at days 0–3 along the WCB trajectories, for the seven boxes shown in Fig. 3.

Box no.	1	2	3	4	5	6	7
After 0 h	11.94	9.66	6.60	11.74	10.15	8.61	8.56
After 24 h	6.08	4.77	2.96	5.61	5.05	4.38	4.57
After 48 h	0.44	0.35	0.24	0.40	0.33	0.33	0.36
After 72 h	0.23	0.20	0.15	0.21	0.18	0.19	0.20

TABLE 4. Fifteen-year climate-mean potential temperature Θ (K) at days 0–3 along the WCB trajectories, for the seven boxes shown in Fig. 3.

Box no.	1	2	3	4	5	6	7
After 0 h	296.0	296.6	305.1	294.8	296.4	292.6	295.3
After 24 h	304.9	303.6	312.4	303.9	305.5	299.0	300.7
After 48 h	317.9	313.6	319.4	316.1	315.8	307.9	310.6
After 72 h	317.0	312.7	318.5	315.2	314.9	306.7	309.6

and 12 g kg^{-1} (Table 3), with the highest values found for the Atlantic and Pacific. Although the WCBs starting in the Indian Ocean and Australia boxes originate mostly over the ocean, too, their initial q is about 20%–30% smaller. This smaller supply with latent energy may be an important reason why they ascend by about 30 hPa less than their Atlantic and Pacific counterparts (see Table 2), similarly to the dependency of the depth of the tropical convection on sea surface temperature and moisture availability (Webster 1994).

The lowest q values are found for Asian WCBs, because of their higher starting altitude. After 48 h the mean q has decreased to about 0.2–0.4 g kg^{-1}, and after 72 h it is further reduced to about 0.2 g kg^{-1} (Table 3), indicating that the initial moisture supply is almost entirely converted into precipitation. We continue our discussion on WCB precipitation in section 5.

The latent heat release due to the water vapor condensation leads to strong diabatic heating and a corresponding increase in Θ along the trajectories. Climate-mean Θ at the starting positions varies between 292 and 297 K, except for Asia, where it is higher (Table 4). After 48 h, Θ values are between 15 and 22 K higher than at the starting point, which matches very well the decrease in q (Table 3), assuming complete conversion of latent into sensible heat. Furthermore, the boxes with the strongest decrease in q also show the strongest increase in Θ. The good match between the decrease in q and increase in Θ also serves as a validation of our trajectory calculations. On the third day, Θ decreases by about 1 K, due to radiational cooling, which is in agreement with the trajectories' average descent. Here q continues to decrease on the third day, because of the averaging over a small number of trajectories that still ascend (decreasing q) and a larger number of already descending trajectories (constant q).

Even though WCB trajectories ascend strongly at the beginning, relatively few of them actually reach the stratosphere by crossing the 2 PV units surface (Table 5). In both hemispheres, the Pacific and Atlantic are the most likely source regions for the intrusion of WCB trajectories (and, thus, ABL air) into the stratosphere. The maxima are found in the North Pacific and North Atlantic, where about 6% of all WCB trajectories cross the 2 PV unit surface within 120 h. Most of the tropopause crossings occur after 2 days, which indicates that the WCB ascent itself is not the reason for the air intruding into the stratosphere, in agreement with our earlier remarks (see section 1).

4. The relationship between cyclones and WCBs

In this section the relationship between the identified WCBs and cyclones is investigated through both a qualitative comparison of their geographical distribution as well as a detailed linking of individual WCB trajectories and cyclones.

a. The cyclone dataset

The cyclone data is taken from a recent climatology for the ERA-15 period of cyclones and anticyclones on a 6-hourly basis (H. Wernli 2003, unpublished manuscript), that defines cyclones as the region bounded by closed contours of sea level pressure (SLP) encircling a SLP minimum. This dataset contains quasi-stationary and moving cyclones. Here, the full cyclone dataset is used as well as a selection of moving cyclones only. Moving cyclones are defined as cyclones that during their life cycle travel at least 1000 km and intensify by more than 10 hPa. These criteria are subjective but efficient to separate typical storm track depressions from quasi-stationary vortices.

Figure 7 shows the frequency distributions for all cyclones (Fig. 7a,c) and for moving cyclones only (Fig. 7b,d). A value of, say, 20 indicates that there is a cyclone at this location in 20% of the considered time instances. The winter cyclone distribution in the NH (Figs. 7c,d) is in very good agreement with other winter climatologies (e.g., Sickmöller et al. 2000, Gulev et al. 2001), showing pronounced maxima in the Atlantic and Pacific storm tracks and a weaker one in the Mediterranean. In the SH we also find a fairly good agreement with the

TABLE 5. Fifteen-year climate-mean percentage of all WCB trajectories that cross the 2 PV units surface, for the seven boxes shown in Fig. 3.

Box no.	1	2	3	4	5	6	7
After 24 h	0.9	0.4	0.2	0.2	0.5	0.6	0.1
After 48 h	0.9	0.8	0.3	0.2	0.4	0.4	0.2
After 72 h	2.9	2.8	1.7	1.3	2.0	2.2	1.6
After 96 h	4.6	4.5	3.0	2.5	3.9	4.2	3.1
After 120 h	5.8	5.8	4.0	3.7	5.3	5.5	4.4

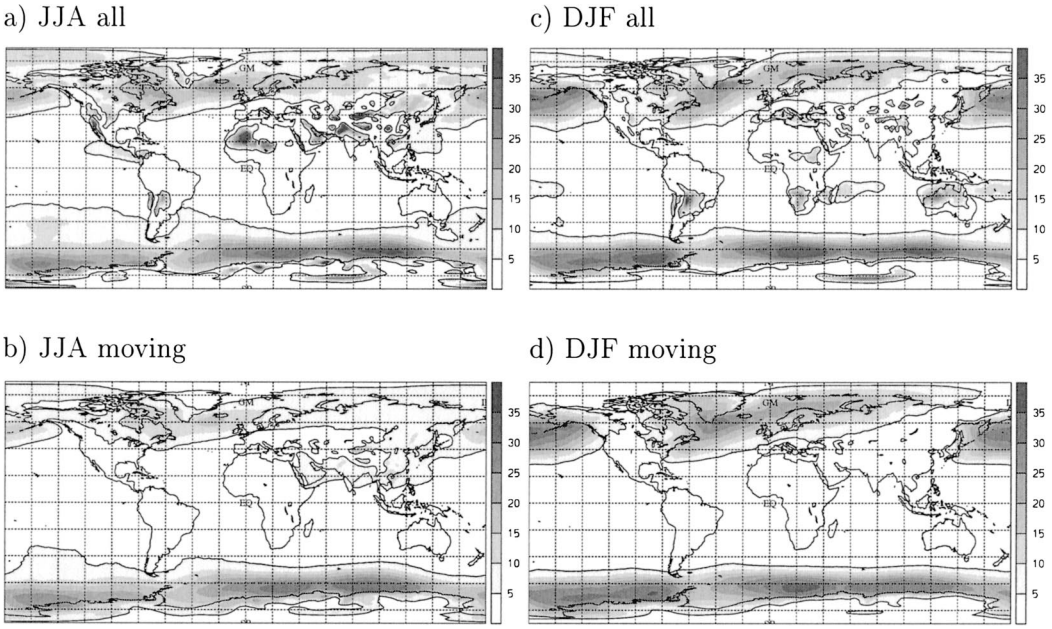

FIG. 7. Fifteen-year climatology of the frequency (in %) of (a) and (c) all cyclones and (b) and (d) moving cyclones only in (a) and (b) JJA and (c) and (d) DJF.

climatologies by Simmonds and Keay (2000b) and Sinclair (1994), though the maxima of quasi-stationary cyclones over land are not always at the same position in the three climatologies and the maximum over South America is completely missing in the Simmonds and Keay (2000b) climatology. The maxima over the continents are mostly heat lows and lee troughs (Sinclair 1994) and do not appear when considering only moving cyclones (compare Figs. 7c and d). In the area adjacent to Antarctica, there are substantial differences found between the three climatologies. Even though they all show very high cyclone frequencies, they do not agree in location and amplitude. Potential reasons for these differences near Antarctica are the proximity of high topography (where the reduction of the surface pressure to sea level pressure might be unreliable and leads to artifacts in the cyclone distribution), and differences in the cyclone identification techniques (H. Wernli 2003, unpublished manuscript).

b. The geographical distribution of cyclones and WCBs

We start with a qualitative comparison of the geographical distribution of cyclones (Fig. 7) and WCB trajectory positions (Fig. 3) in JJA and DJF, the seasons with the largest differences in the cyclone distribution. The seasonal cycle of the cyclone frequency is very pronounced in the NH (with a clear maximum in DJF) and much weaker in the SH, in agreement with the WCB climatology. On the NH, during DJF there is a good correspondence between the WCB trajectory positions after 24–48 h (Figs. 3f,g) and the cyclones over the North Atlantic and North Pacific (Figs. 7c,d). The WCB starting points (Fig. 3e) are located typically in the warm sector south of the cyclone centers, in agreement with the conveyor belt model and the case study shown in Fig. 2. During JJA both cyclones and WCBs occur over the eastern Asian continent. On the SH, the agreement is less good: cyclones occur mainly along the coast of Antarctica (near 55°–70°S), whereas the identified trajectories are situated farther equatorward (30°–60°S). The pronounced maximum of WCB trajectories over and in the lee of South America (in particular during DJF) corresponds to a peak in the distribution of quasi-stationary cyclones (Figs. 7a,c; see also Vera et al. 2002).

In summary, our qualitative considerations indicate that cyclones and WCB trajectories match very well in the NH, especially during winter, and less well in the SH. This points to a systematic difference of cyclone life cycles in the two hemispheres (see below).

c. A comparison of individual cyclones and WCBs

For a detailed comparison of individual cyclones and WCB trajectories, we developed an algorithm to check at every time whether there is (a) a cyclone center within a certain distance from a WCB, and (b) whether there is at least one WCB trajectory within a certain distance of a cyclone center. The first analysis is important as an a posteriori justification for referring to the identified trajectories as WCBs. The second analysis provides information on how many cyclones actually are associated with WCBs, and whether this relationship shows geographical and/or seasonal variability. For computational

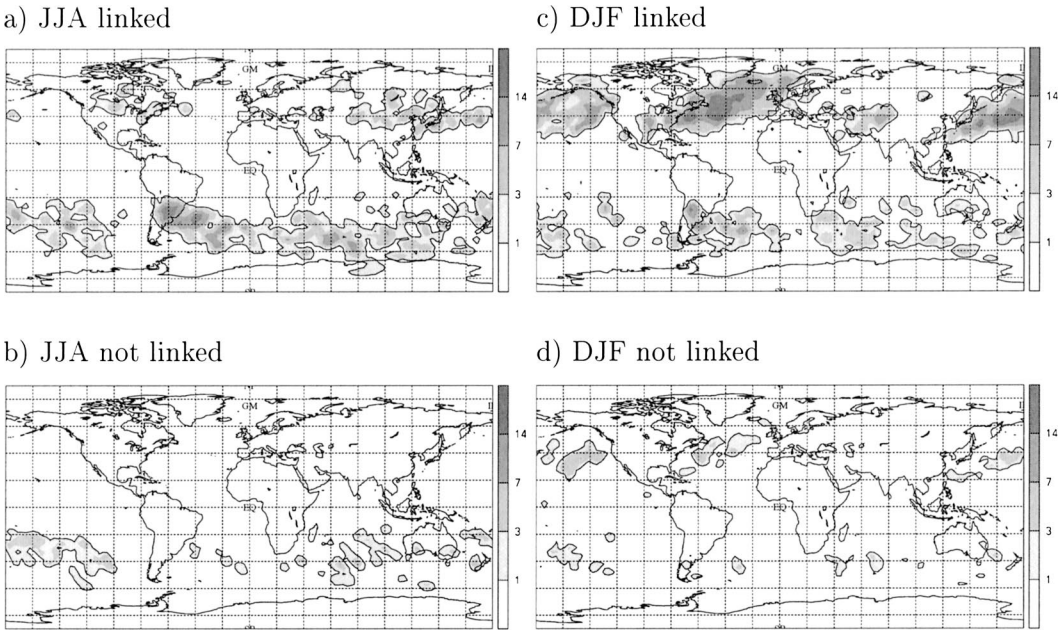

FIG. 8. Link between identified WCB trajectories and cyclones for (a) and (b) JJA 1992 and (c) and (d) DJF 1992. (a) and (c) The trajectory positions after 24 h of the trajectories that get closer than 1000 km to the center of a cyclone during their ascent phase of 48 h; (b) and (d) those that do not pass within 1000 km of a cyclone center. The values correspond to the total number of linked/not linked trajectories during the 3-month period per 10^5 km^2.

reasons this detailed investigation is limited to a single year (1992).

For this analysis the WCB positions are considered only after 24 h (i.e., during the ascent phase, when they are closest to the cyclone center), and a threshold radius of 1000 km was chosen to decide about the proximity of cyclones and WCBs. This value corresponds to a typical radius of a mature cyclone and the case study (Fig. 2a) indicates that it serves well to decide whether the two features are linked or not.

Figure 8 shows the positions after 24 h of the trajectories that are linked with a moving or quasi-stationary cyclone (panels a, c) and of those that are not (panels b, d). Comparing the number of WCBs that could be linked by our algorithm (Fig. 8) to the total number of WCBs gives us the percentage of WCBs that occur in the vicinity of a cyclone. Clearly, the dominant part of our identified trajectories (90%–100% in the NH, 77%–86% in the SH) occur in the vicinity of a cyclone, and only a small percentage might be unrelated to a SLP minimum (or ascend farther away from the cyclone center). However, note that many WCB trajectories are related to quasi-stationary cyclones, especially in the SH (e.g., over South America).

The reverse comparison (Fig. 9), carried out with moving cyclones, reveals interesting seasonal and hemispheric asymmetries: during NH winter the major part (60%, Fig. 9c) of the moving cyclones are associated with at least one WCB trajectory. During NH summer this percentage is much smaller (28%). In the SH only about 35% of the cyclones are accompanied by WCBs, irrespective of the season. In particular, the cyclones that travel along the coast of Antarctica are almost always devoid of WCB trajectories (Fig. 9b,d). This points to a significant difference in the role of moist processes for extratropical cyclone development in the two hemispheres. In the NH and during winter, WCBs (as identified in this study) are prominent and frequent features of midlatitude depressions and underline the importance of latent heat release for the intensification of these systems. However, the most frequent SH cyclones occurring near 60°S close to Antarctica are associated with weaker or no WCBs and are therefore less influenced by diabatic processes. This hemispheric asymmetry is in qualitative agreement with the less frequent occurrence of rapid cyclone development in the SH compared to the NH (Lim and Simmonds 2002).

It would be interesting to confirm this identified interhemispheric difference of the link of WCBs and cyclones using independent data. Since WCBs are associated with cloud formation, we used data from the International Satellite Cloud Climatology Project (ISCCP; Rossow et al. 1996; Rossow and Schiffer 1999; available online at http://isccp.giss.nasa.gov/products/browsed2.html) to validate our hypothesis that prominent WCBs are missing in the cyclones along the coast of Antarctica. In particular, we expect high clouds to be very frequent in areas where we identify many WCB trajectories, but to be less frequent in the cyclone maximum around Antarctica, where we do not see many WCBs.

In both hemispheres there is an excellent agreement

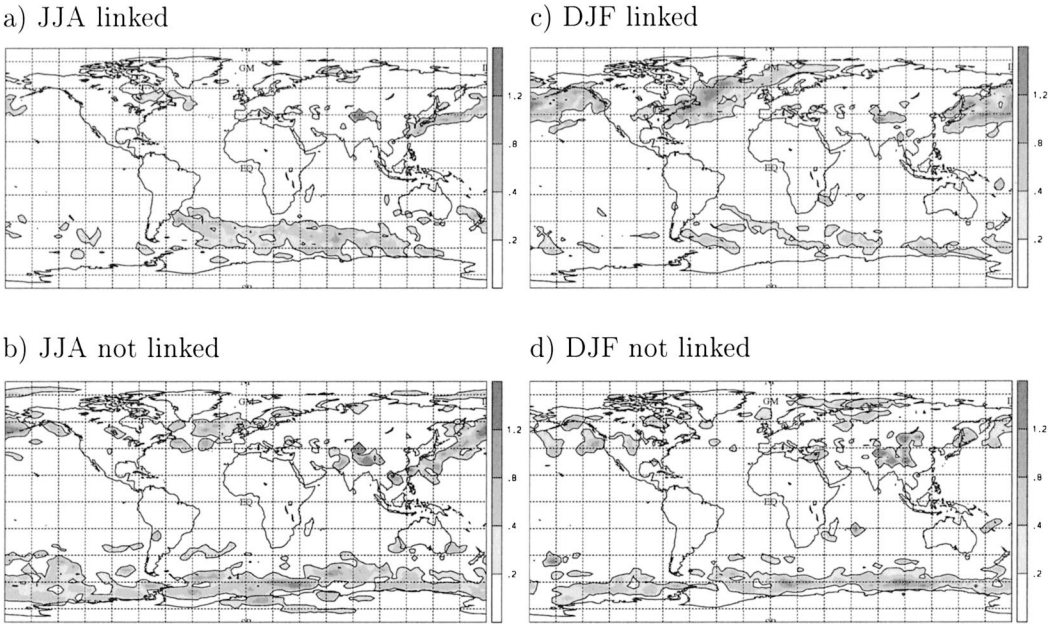

FIG. 9. The reverse of Fig. 8: Link between moving cyclones and identified WCB trajectories for (a) and (b) JJA 1992 and (c) and (d) DJF 1992. (a) and (c) Cyclone centers that are closer than 1000 km to at least one ascending WCB trajectory; (b) and (d) cyclone centers that are not passed within 1000 km by any WCB trajectory. The values correspond to the total number of linked/not linked cyclone centers during the 3-month period per 10^5 km^2.

between the distribution of high clouds (Figs. 10b,d) outside the Tropics, and WCB trajectory positions after 24–48 h (cf. Fig. 3). In the NH, there is also a good correspondence with the occurrence of cyclones (compare with Fig. 7). In the SH, however, the high cloud distribution matches well only with the WCB distribution, whereas there are relatively few high clouds in the cyclone maximum around Antarctica, at least in DJF (unfortunately, no high cloud data are available at high southern latitudes in JJA).

Instead, we see that these cyclones are associated with the highest frequency of middle clouds on earth (Figs. 10a,c). This confirms our expectation that these SH cyclones are less influenced by diabatic processes than their counterparts in the NH. They nevertheless lead to strong cloud formation, but at lower levels in the atmosphere than other cyclones. They also produce less precipitation (see below).

5. WCBs and precipitation

Figures 11a and 11b show the global distribution of annual precipitation obtained from observations of the Global Precipitation Climatology Project (GPCP) (Susskind et al. 1997) and from the ERA-15 dataset (convective plus large-scale precipitation taken from the 6-h first guesses), respectively. ERA-15 reproduces the basic patterns seen in the precipitation observations. However, the tropical precipitation maximum at the intertropical convergence zone is overestimated by ERA-15, especially over South America, whereas the maxima in the midlatitude stormtracks are somewhat underestimated. These are known features of ERA-15 and also of other reanalysis projects (Stendel and Arpe 1999), which point toward excessive convective versus too small large-scale precipitation. Also, precipitation over some mountain ranges, such as the Andes, is overestimated by ERA-15.

As explained in section 2, global precipitation fields can be calculated from the decrease in q along the trajectories. We assume that all precipitation falls within 3 days after a trajectory's start and that q decreases monotonously along a trajectory, not an unlikely assumption for trajectories starting in the boundary layer (we ignore the occasional occurrences of increasing q along a trajectory segment). These are certainly subjective assumptions and our trajectory-derived precipitation maps suffer also from the fact that trajectories were started at one level and once a day only. Furthermore, positions and values of q were stored only every 24 h along the trajectories, rendering the spatial attribution of precipitation difficult. Nevertheless, we find that our method works surprisingly well in reconstructing the ERA-15 precipitation fields, showing the expected maxima in the Tropics and midlatitude storm tracks (Fig. 11c). Precipitation maxima in mountain regions (e.g., at the North American west coast or at the southern end of the Andes) are captured quite well, too, but are smeared out over large areas because of the low resolution of the trajectory model output (averaging over 24 h). There are even some features that appear to be in better agreement with the precipitation observa-

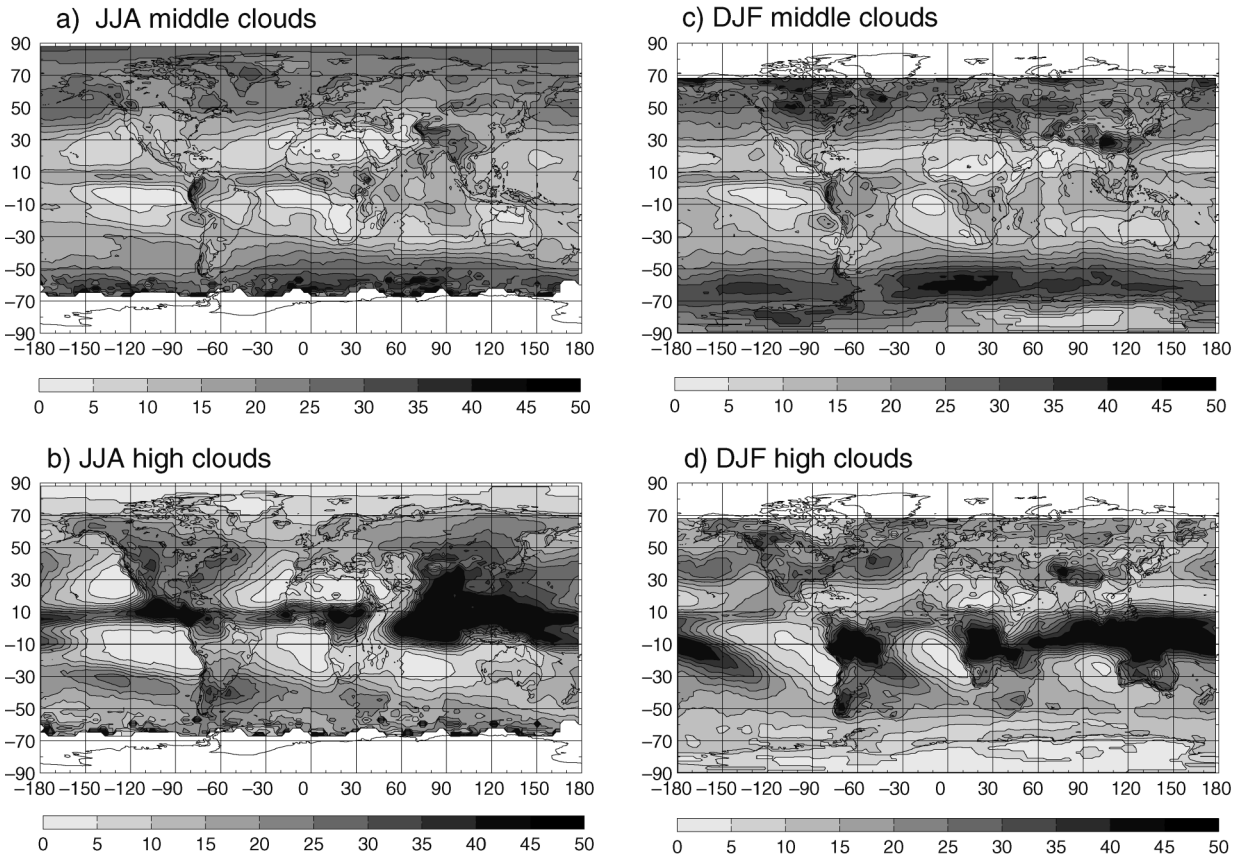

FIG. 10. Average cloud cover (%) for middle clouds in (a) JJA, (c) middle clouds in DJF, (b) high clouds in JJA, and (d) high clouds in DJF from the ISCCP climatology for the years 1983–2001. High clouds are defined in the ISCCP climatology as clouds occurring above 440 hPa (cirrus, cirrostratus, and deep convection), middle clouds are those between 680 and 440 mbar (covering altocumulus, altostratus, and nimbostratus). Cloud data are missing poleward of approximately 65° in the respective winter season (white areas).

tions (Fig. 11a) than the ERA-15 precipitation itself (Fig. 11b). For instance, the precipitation maximum in the North Atlantic stormtrack extends farther north to Iceland, and the precipitation maximum south of Australia appears to be at the correct latitude (60°S), whereas ERA-15 puts it too far north (50°S). This may be fortuitous, but it should be noted that, in principle, the trajectory method may also produce precipitation fields that are superior to the ERA-15 precipitation. The trajectory method uses only fields of q and the winds, which both benefit from the continuous assimilation of observations, whereas the ERA-15 precipitation is a purely prognostic product. This may be explored further in a future study. Here it is sufficient to note that the trajectory technique is capable of re-constructing approximately the basic precipitation patterns and magnitudes. We may thus proceed to separate WCB precipitation from precipitation due to other processes.

Figure 11d shows the 15-yr mean distribution of WCB annual precipitation. The WCB precipitation patterns resemble closely those of the WCB trajectory paths during the first 48 h (Fig. 3). Most of the WCB precipitation falls over the first half of the storm tracks, where the WCBs ascend strongly, whereas relatively little WCB precipitation falls over the ends of the storm tracks, where WCBs often turn anticyclonically. These are well-known features of the global precipitation distribution (compare Figs. 11a–c), which points toward the importance of the WCB mechanism for producing them. In contrast, there is much less WCB precipitation around Antarctica, because of the relative rarity of WCBs there. In the GPCP data (Fig. 11a) and in the ERA-15 precipitation (Fig. 11b), we also see that there is less precipitation ringing Antarctica than there is in the NH stormtracks, even though cyclones are much more frequent around Antarctica (Fig. 7). A comparison of Fig. 11a (or Fig. 11b) and Fig. 7 shows that precipitation per sub-Antarctic cyclone is only about 50% of that per NH stormtrack cyclone (note that if the smaller mean sizes of cyclones around Antarctica were accounted for, the difference would be even larger). This confirms that sub-Antarctic cyclones are less influenced by diabatic processes than cyclones in the NH.

If we compare WCB with non-WCB trajectories, we find that a WCB trajectory produces about twice as much precipitation as an average trajectory starting from

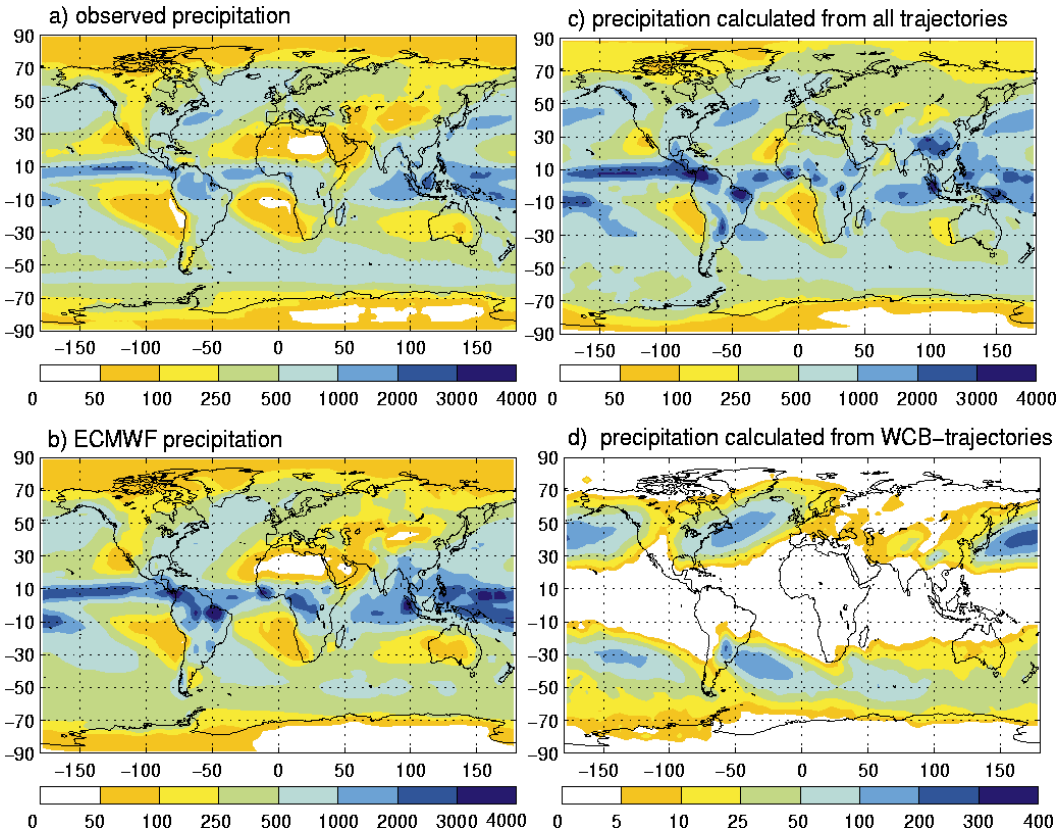

FIG. 11. Global distribution of the annual precipitation (mm) from different sources: (a) precipitation observations obtained from the GPCP (covering the time period from Jan 1979 to Jul 2001), (b) 15-yr average annual precipitation (convective plus large-scale precipitation) in the ERA-15 dataset, (c) 15-yr average annual precipitation calculated from the decrease in q using all trajectories, (d) 15-yr average WCB precipitation calculated from the decrease in q using WCB trajectories only.

the same position, and about four (six) times as much precipitation as the global (extratropical) average trajectory starting from 500 m AGL (note that trajectories starting in WCB source regions produce systematically more precipitation than the global average). Nevertheless, WCB precipitation contributes only about 6%–10% (11%–17%) to the total annual (winter) precipitation in the storm track precipitation maxima (compare Figs. 11c and 11d for the annual values) and only about 2% of the global annual precipitation. These percentages increase by a factor of nearly 3 when the ascent criterion is reduced from 60% to 40% (Table 1). In the case study (section 2) we furthermore have seen that, if all trajectories ascending to above 850 hPa in the vicinity of a WCBs' core are considered, four times more precipitation was produced than by the WCB core alone. If we apply this (conservative) factor 4, we find that 24%–40% (44%–72%) of the total annual (winter) precipitation in the storm track precipitation maxima and about 8% of the global annual precipitation are due to WCBs.

If we compare the precipitation produced by WCB cores identified with our standard criteria (and, upscaling with a factor 4, by WCBs totally) with a precipitation value for cyclones taken from the literature (see Table 1), we find that WCB cores (WCBs) account for about 8% (32%) of the global precipitation in extratropical cyclones. These values are consistent with our own similar estimates above and confirm the important role of WCB precipitation in cyclones (see, e.g., Browning 1990). However, globally, mesoscale convective systems and thunderstorms produce more precipitation (Table 1).

6. Interannual variability

Figure 12 shows time series of the monthly mean WCB mass fluxes in the seven boxes defined in Fig. 3 over the 15-yr period. In the NH there is a clear annual cycle with a winter maximum that is repeated every year (except for Asia). In the SH, the annual cycle is more complicated, often featuring two independent maxima, the relative magnitude of which varies from year to year. We have already seen that this is related to the frequent association of WCBs with quasi-stationary cyclones in the SH (particularly over South America and South Africa), whose seasonal cycle peaks later in the year than that of moving cyclones.

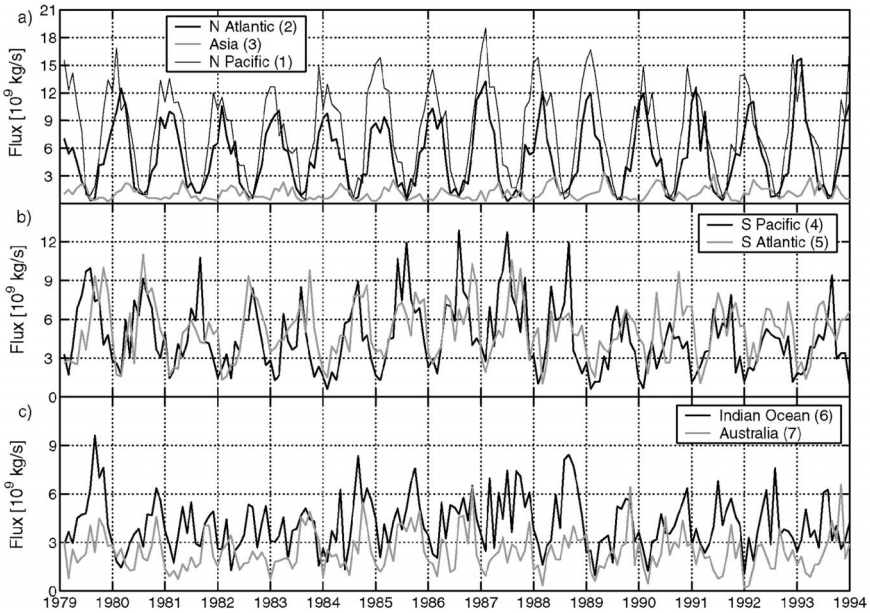

FIG. 12. Fifteen-year time series of monthly WCB mass fluxes (10^9 kg s^{-1}) for the (a) NH, (b) eastern SH, and (c) western SH for the seven boxes shown in Fig. 3.

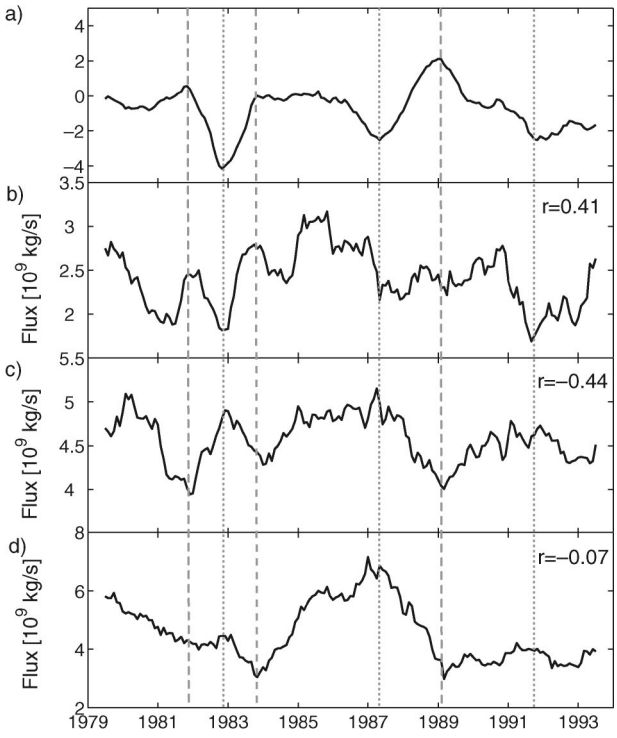

FIG. 13. Fifteen-year time series of the (a) SO index, (b) WCB mass fluxes (10^9 kg s^{-1}) for the Australian (7) box, (c) the South Atlantic (5) box, and (d) the South Pacific (4) box, all smoothed with a 12-month running mean. Dashed (dotted) vertical lines are drawn through pronounced maxima (minima) of the SO index.

a. El Niño–Southern Oscillation

Interannual variations of WCB frequencies are typically of the order of about 30%. They are generally greater in the SH than in the NH, and are particularly large in the South Pacific (see also Fig. 4), where in some years they may exceed 100%. In order to explain these interannual variations we investigated the relationship of WCB frequencies with two important modes of climate variability, the El Niño–Southern Oscillation (ENSO), and the North Atlantic Oscillation (NAO). ENSO is a joint phenomenon of the ocean and the atmosphere. While El Niño is a recurring anomaly of the sea surface temperatures (SST) in the tropical Pacific, the Southern Oscillation (SO) represents a seesaw of sea level pressure anomalies between Tahiti and Darwin (Walker and Bliss 1932, 1937). Indices for both phenomena are closely correlated, but as we are concerned here with the atmosphere, we use the SO index data from the Climate Prediction Center, Maryland (available online at ftp://ftp.ncep.noaa.gov/pub/cpc/wd52dg/data/indices/soi), for our analysis. The SO index is negative during El Niño events and positive during La Niña events (e.g., Trenberth and Caron 2000).

First, we performed a correlation analysis between the SO index and the WCB frequencies in our seven boxes, all smoothed with a 12-month running mean to remove the annual cycle. The smoothed time series and correlation coefficients for three boxes are shown in Fig. 13. The highest correlation coefficients, statistically significant at the 99% confidence level, are found for the South Atlantic (-0.44) and Australia (0.41), whereas no clear correlation exists for the South Pacific, the region with the highest variation of WCB frequency.

TABLE 6. Winter months and their associated NAO index used for constructing the low and high NAO index ensembles, respectively.

Low NAO			High NAO		
Month	Year	Index	Month	Year	Index
1	1987	−4.6	1	1983	3.5
1	1985	−3.9	1	1984	4.1
1	1979	−3.6	1	1990	4.3
2	1986	−3.9	2	1992	2.7
2	1983	−1.8	2	1989	4.1
2	1985	−1.8	2	1990	4.7
12	1989	−3.8	12	1986	2.7
12	1987	−2.7	12	1993	3.0
12	1981	−2.3	12	1982	3.3

Both the positive correlation for Australia and the negative correlation for the South Atlantic are likely the result of varying SST variations in these regions. SSTs around Australia (in the South Atlantic) are higher (lower) than normal for a positive SO index (Alexander et al. 2002), leading to enhanced (reduced) latent heat release into the atmosphere and, because of the strong dependence of cyclogenesis on diabatic processes, more frequent (less frequent) WCBs. The lack of correlation for the South Pacific is surprising, as this region is closest to the center of action of the ENSO phenomenon. Two reasons may explain this negative result: First, our South Pacific box covers a large region, with partly opposing SST anomalies. Second, problems occurred in the ERA-15 production over the western Amazon basin, which became too hot and dried out between 1980 and 1987 (Gibson et al. 1999). It is, thus, possible that the large peak in WCB frequency in the year 1986 is artificial and related to this problem in the reanalysis data. For subperiods (e.g., from 1981 to 1984, when the correlations in the other boxes are very high, too) there indeed appears to be an anticorrelation between WCB frequency in the South Pacific box and the SO index. In the North Pacific, there is also a positive correlation (0.30) between the SO index and WCB frequency, in agreement with the associated SST anomalies.

b. North Atlantic Oscillation

The NAO is an important reason for climate variability in the NH (Hurrell 1995). The NAO is characterized by a variation of mean atmospheric mass distribution between the Arctic and the subtropical Atlantic and dictates climate variability from the eastern seaboard of North America to Siberia and from the Arctic to the subtropical Atlantic, especially in winter. The NAO index is expressed as the difference of normalized pressures between Lisbon, Portugal, and Stykkishólmur, Iceland (Hurrell 1995). High values of the NAO index are associated with a strengthening of the North Atlantic storm track with well-developed westerlies (Rogers 1997), leading to relatively warm winters over Europe and cold conditions in the northwestern Atlantic. Wetter than normal conditions prevail in northern Europe and dry winters occur in southern Europe during phases of high NAO index (Hurrell and van Loon 1997). During winters with high NAO index, the North Atlantic cyclone density shifts northward and is associated with more stationary cyclones (Sickmöller et al. 2000). It may, thus, be expected that the NAO influences the WCB distribution.

Since the NAO is most pronounced in winter, we compare our WCB distribution with the NAO index for DJF only. We constructed two ensemble datasets consisting of the three Decembers, three Januaries, and three Februaries featuring the highest and the lowest monthly values of the NAO index, respectively (see Table 6), out of the 15 values available for each month during the period 1979–93. The NAO index data were provided by the Climate Analysis Section, National Center for Atmospheric Research, Boulder, via the internet (available online at http://www.cgd.ucar.edu/~jhurrell/nao.html).

On average, WCBs in the North Atlantic are about 12% more frequent for the high NAO index ensemble than for the low index ensemble. Figure 14 shows the geographical distribution of WCB trajectory starting points (WCB inflow) and trajectory positions after 2 days (WCB outflow) in dependence of the NAO index. Panels (a, d) and (b, e) compare the WCB position frequencies for the low and high NAO index ensembles, while panels (c, f) present correlations between the NAO index and WCB inflow (c) and outflow (f) frequency, respectively. The region with maximum WCB inflow extends farther to the northeast for the high NAO index ensembles (Fig. 14b) than for the low NAO index ensemble (Fig. 14a). Even though the inflow differences between the two ensembles appear to be relatively small, the dependence of the WCB inflow patterns on the NAO index is statistically significant (Fig. 14c). This is even more true for the WCB outflow patterns (Fig. 14f): In the low NAO case (Fig. 14d) WCB outflow occurs most frequently south of Greenland and Iceland, whereas in the high NAO case (Fig. 14e) it is most frequent between Iceland and Scandinavia, about 10° farther north and 20° farther east than in the low NAO case. Thus, WCB transport is much faster and is directed more toward the north during the positive phase of the NAO, in agreement with the strengthening and northward shift of the storm track (Rogers 1997). The wetter than normal conditions in northwestern Europe during high NAO phases are, therefore, related to the enhanced frequency of WCBs and the drier than normal conditions in southern Europe correspond to a reduced frequency of WCBs.

7. Conclusions

In this study we have developed the first detailed climatology of WCBs. The basis was a dataset of daily trajectories starting on a global grid at 500 m AGL, which were calculated using 15 yr (1979–93) of reanalysis data from ECMWF. WCBs were identified by

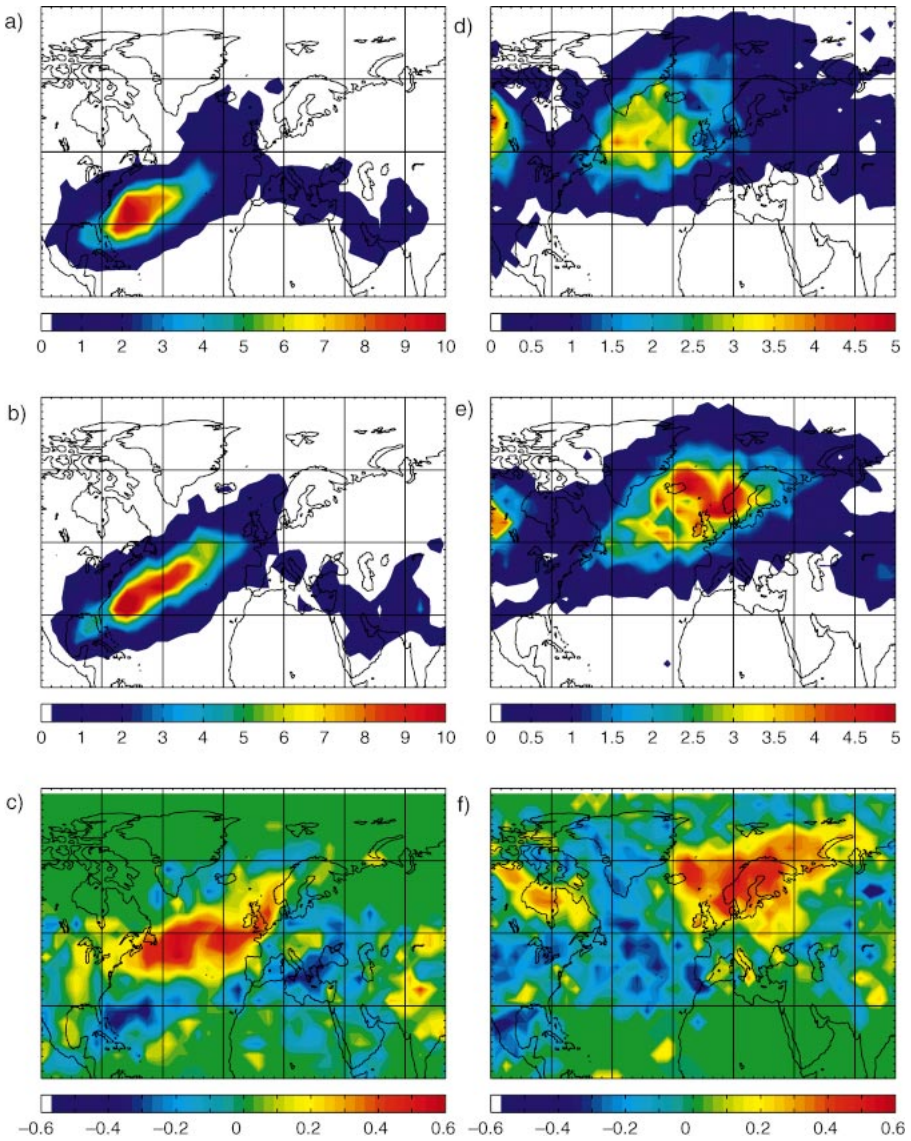

FIG. 14. The relation between WCBs and the NAO index: Spatial distribution of the frequency (in percent of all trajectories) of (a) and (b) WCB trajectory starting points and (d) and (e) WCB trajectory positions after 48 h for ensembles of the nine winter months (three Dec, three Jan, three Feb) associated with the (a) and (d) lowest and the (b) and (e) highest values of the NAO index during the 15-yr period from 1979–93. Correlation analysis was performed for each grid cell between WCB frequency and NAO index (for 15 winters). (c) and (f) Correlation coefficients of the NAO index and WCB frequency for (c) WCB trajectory starting points and (f) WCB trajectory positions after 48 h for all winter months. Correlation coefficients greater (smaller) than 0.29 (−0.29) are statistically significant on the 95% confidence level.

searching for trajectories that, during a period of 2 days, ascended by at least 60% of the zonally and climatologically averaged tropopause height and traveled more than 10° longitude to the east and more than 5° latitude to the north. With these criteria, only the cores of reasonably strong WCBs are classified. The WCB climatology was compared with a new cyclone climatology, cloud and precipitation observations, and with indices for climate variability. The major findings from this work are the following:

1) The typical timescale of a WCB is 2 days, during which it ascends from the ABL to the upper troposphere. After this period, WCB trajectories typically turn anticyclonically and descend by about 20 hPa day^{-1}.
2) WCB starting points are most frequent between approximately 25° and 45°N and 20° and 45°S. In the NH, there are two distinct maxima east of North America and east of Asia, whereas very few WCBs originate from Eurasia and western North America.

In the SH, there is much less zonal variability, and WCB starting locations are located about 5° of latitude closer to the equator than in the NH.

3) WCBs occur more frequently during the winter than during the summer. The seasonal variation is stronger in the NH than in the SH. In the NH, WCBs are almost an order of magnitude more frequent in January than in July.
4) WCB mass fluxes are sensitive to the WCB selection criteria, but are generally 20%–60% higher in the SH than in the NH. Our criteria identify the particularly strong WCB cores; the total mass flux of a WCB is about an order of magnitude higher than that of its core. WCB mass fluxes across 850 hPa are about a third of the total upward fluxes in extratropical cyclones found in other studies. WCB mass fluxes are comparable to mass fluxes in mesoscale convective systems and thunderstorms and clearly exceed those of tropical cyclones and mesoscale convective complexes.
5) The climate-mean specific humidity at WCB starting points in different regions varies from 7 to 12 g kg^{-1}. This moisture is almost entirely converted to precipitation, leading to an increase of potential temperature of 15–22 K.
6) About 6% of all WCB trajectories reach the stratosphere within 5 days. However, the crossing of the tropopause normally occurs only after the WCB's 2 days ascent.
7) Most (90%–100% in the NH, 77%–86% in the SH) of the WCBs were found within 1000 km of a cyclone center. The reverse comparison revealed that moving cyclones are normally (more than 60% of them) accompanied by a strong WCB only in the NH winter. In the SH, many of the WCBs are related to quasi-stationary cyclones at rather low latitudes (e.g., over South America). On the other hand, practically no strong WCBs are found around Antarctica, where cyclones are globally most frequent. These cyclones are, thus, less influenced by diabatic processes, in agreement with their smaller growth rates. The large interhemispheric differences of the relationship between cyclones and strong WCBs also reveal considerable differences between the general circulation in the two hemispheres.
8) Outside the Tropics, there is excellent agreement between the distribution of WCBs and the occurrence of high clouds obtained from a cloud climatology. The cyclones around Antarctica, which are devoid of WCBs, are also less associated with high clouds than cyclones in other regions.
9) Using a technique to diagnose precipitation from the decrease of specific humidity along ascending trajectories, we could approximately reconstruct global precipitation fields.
10) Over the course of 3 days, a WCB trajectory produces, on average, about twice as much precipitation as the average trajectory starting from the same location, and about four (six) times as much precipitation as a global (extratropical) average trajectory starting from 500 m AGL.
11) In the winter, there is a highly significant correlation between the North Atlantic Oscillation and the WCB distribution in the North Atlantic: In months with a high NAO index, WCBs are about 12% more frequent and their outflow occurs about 10° latitude farther north and 20° longitude farther east than in months with a low NAO index. The differences in the WCB inflow regions are relatively small between the two NAO phases.
12) WCBs occur more (less) frequent around Australia (in the South Atlantic) for high phases of the Southern Oscillation.

Acknowledgments. We thank two anonymous reviewers for their detailed comments, which helped shape the final version of this paper. This study was co-funded by the German Federal Ministry for Education and Research within the Atmospheric Research Program 2000 (AFO 2000) as part of the projects CARLOTTA and CONTRACE, and by the European Commission under Contract EVK2-CT-2001-00112 (project PARTS). ECMWF and the German Weather Service are acknowledged for permitting access to the ECMWF archives.

REFERENCES

Alexander, M. A., I. Blade, M. Newman, J. R. Lanzante, N. C. Lau, and J. D. Scott, 2002: The atmospheric bridge: The influence of ENSO teleconnections on air–sea interaction over the global oceans. *J. Climate,* **15,** 2205–2231.

Arnold, F., J. Schneider, K. Gollinger, H. Schlager, P. Schulte, D. E. Hagen, P. D. Whitefield, and P. van Velthoven, 1997: Observation of upper tropospheric sulfur dioxide- and acetone-pollution: Potential implications for hydroxyl radical and aerosol formation. *Geophys. Res. Lett.,* **24,** 57–60.

Bethan, S., G. Vaughan, C. Gerbig, A. Volz-Thomas, H. Richer, and D. A. Tiddeman, 1998: Chemical air mass differences near fronts. *J. Geophys. Res.,* **103,** 13 413–13 434.

Bjerknes, V., 1910: Synoptical representation of atmospheric motions. *Quart. J. Roy. Meteor. Soc.,* **36,** 167–286.

Browning, K. A., 1990: Organization of clouds and precipitation in extratropical cyclones. *Extratropical Cyclones: The Erik H. Palmén Memorial Volume,* C. Newton and E. Holopainen, Eds., Amer. Meteor. Soc., 129–153.

——, 1999: Mesoscale aspects of extratropical cyclones: An observational perspective. *The Life Cycles of Extratropical Cyclones,* M. A. Shapiro and S. Gronas, Eds., Amer. Meteor. Soc., 265–283.

——, M. E. Hardman, T. W. Harrold, and C. W. Pardoe, 1973: Structure of rainbands within a mid-latitude depression. *Quart. J. Roy. Meteor. Soc.,* **99,** 215–231.

Carlson, T. N., 1980: Airflow through midlatitude cyclones and the comma cloud pattern. *Mon. Wea. Rev.,* **108,** 1498–1509.

——, 1998: *Mid-Latitude Weather Systems.* Amer. Meteor. Soc., 507 pp.

Cohen, R. A., and C. W. Kreitzberg, 1997: Airstream boundaries in numerical weather simulations. *Mon. Wea. Rev.,* **125,** 168–183.

Cooper, O. R., and Coauthors, 2001: Trace gas signatures of airstreams within North Atlantic cyclones: Case studies from the North Atlantic Regional Experiment (NARE '97) aircraft intensive. *J. Geophys. Res.,* **106,** 5437–5456.

——, and Coauthors, 2002: Trace gas composition of midlatitude cyclones over the western North Atlantic Ocean: A conceptual model. *J. Geophys. Res.,* 4056, **107**, doi:10.1029/2001JD000901.

Cotton, W. R., G. D. Alexander, R. Hertenstein, R. L. Walko, R. L. McAnelly, and M. Nicholls, 1995: Cloud venting—A review and some new global annual estimates. *Earth Sci. Rev.,* **39,** 169–206.

Davis, C. A., M. T. Stoelinga, and Y.-H. Kuo, 1993: The integrated effect of condensation in numerical simulations of extratropical cyclogenesis. *Mon. Wea. Rev.,* **121,** 2309–2330.

Gibson, J. K., P. Kallberg, S. Uppala, A. Hernandez, A. Nomura, and E. Serrano, 1999: ERA-15 Description. ECMWF re-analysis project report series 1, version 2, ECMWF, Reading, United Kingdom, 77 pp.

Gulev, S. K., O. Zolina, and S. Grigoriev, 2001: Extratropical cyclone variability in the Northern Hemisphere winter from the NCEP/NCAR reanalysis data. *Climate Dyn.,* **17,** 795–809.

Harrold, T. W., 1973: Mechanisms influencing distribution of precipitation within baroclinic disturbances. *Quart. J. Roy. Meteor. Soc.,* **99,** 232–251.

Hoskins, B. J., and K. I. Hodges, 2002: New perspectives on the Northern Hemisphere winter storm tracks. *J. Atmos. Sci.,* **59,** 1041–1061.

——, M. E. McIntyre, and A. W. Robertson, 1985: On the use and significance of isentropic potential vorticity maps. *Quart. J. Roy. Meteor. Soc.,* **111,** 877–946.

Hurrell, J. W., 1995: Decadal trends in the North Atlantic Oscillation: Regional temperatures and precipitation. *Science,* **269,** 676–679.

——, and H. Van Loon, 1997: Decadal variations in climate associated with the North Atlantic Oscillation. *Climatic Change,* **36,** 301–326.

Iskenderian, H., 1988: Three-dimensional airflow and precipitation structure in a nondeepening cyclone. *Wea. Forecasting,* **3,** 18–32.

Kästner, M., R. Meyer, and P. Wendling, 1999: Influence of weather conditions on the distribution of persistent contrails. *Meteor. Appl.,* **6,** 261–271.

Kuo, Y.-H., M. A. Shapiro, and E. G. Donall, 1991: The interaction between baroclinic and diabatic processes in a numerical simulation of a rapidly intensifying extratropical marine cyclone. *Mon. Wea. Rev.,* **119,** 368–384.

Lim, E. P., and I. Simmonds, 2002: Explosive cyclone development in the Southern Hemisphere and a comparison with Northern Hemisphere events. *Mon. Wea. Rev.,* **130,** 2188–2209.

Martin, J. E., 1998: The structure and evolution of a continental winter cyclone. Part II: Frontal forcing of an extreme snow event. *Mon. Wea. Rev.,* **126,** 329–348.

Massacand, A. C., H. Wernli, and H. C. Davies, 2001: Influence of upstream diabatic heating upon an Alpine event of heavy precipitation. *Mon. Wea. Rev.,* **129,** 2822–2828.

Mullen, S. L., 1987: Transient eddy forcing of blocking flows. *J. Atmos. Sci.,* **44,** 3–22.

Newell, R. E., N. E. Newell, Y. Zhu, and C. Scott, 1992: Tropospheric rivers? A pilot study. *Geophys. Res. Lett.,* **19,** 2401–2404.

Peixoto, J. P., and A. H. Oort, 1992: *Physics of Climate.* American Institute of Physics, 520 pp.

Pomroy, H. R., and A. J. Thorpe, 2000: The evolution and dynamical role of reduced upper-tropospheric potential vorticity in intensive observing period one of FASTEX. *Mon. Wea. Rev.,* **128,** 1817–1834.

Rogers, D. C., P. J. DeMott, S. M. Kreidenweiss, and Y. Chen, 1998: Measurements of ice nucleating aerosols during SUCCESS. *Geophys. Res. Lett.,* **25,** 1383–1386.

Rogers, J. C., 1997: North Atlantic storm track variability and its association to the North Atlantic Oscillation and climate variability of northern Europe. *J. Climate,* **10,** 1635–1647.

Rossow, W. B., and R. A. Schiffer, 1999: Advances in understanding clouds from ISCCP. *Bull. Amer. Meteor. Soc.,* **80,** 2261–2287.

——, A. W. Walker, D. E. Beuschel, and M. D. Roiter, 1996: International Satellite Cloud Climatology Project (ISCCP) documentation of new cloud datasets. World Climate Research Programme (ICSU and WMO) WMO/TD 737, 115 pp.

Sanders, F., and J. R. Gyakum, 1980: Synoptic-dynamic climatology of the bomb. *Mon. Wea. Rev.,* **108,** 1589–1606.

Schultz, D. M., 2001: Reexamining the cold conveyor belt. *Mon. Wea. Rev.,* **129,** 2205–2225.

Sickmöller, M., B. Blender, and K. Fraedrich, 2000: Observed winter cyclone tracks in the Northern Hemisphere in re-analysed ECMWF data. *Quart. J. Roy. Meteor. Soc.,* **126,** 591–620.

Simmonds, I., and K. Keay, 2000a: Variability of Southern Hemisphere extratropical cyclone behaviour, 1958–97. *J. Climate,* **13,** 550–561.

——, and ——, 2000b: Mean Southern Hemisphere extratropical cyclone behavior in the 40-year NCEP–NCAR reanalysis. *J. Climate,* **13,** 873–885.

Sinclair, M. R., 1994: An objective cyclone climatology for the Southern Hemisphere. *Mon. Wea. Rev.,* **122,** 2239–2256.

Stendel, M., and K. Arpe, 1999: Evaluation of the hydrological cycle in reanalyses and observations. ECMWF Re-Analysis Project Report Series 6, ECMWF, 53 pp.

Stewart, R. E., K. K. Szeto, R. F. Reinking, S. A. Clough, and S. P. Ballard, 1998: Midlatitude cyclonic cloud systems and their features affecting large scales and climate. *Rev. Geophys.,* **36,** 245–273.

Stoelinga, M. T., 1996: A potential vorticity-based study of the role of diabatic heating and friction in a numerically simulated baroclinic cyclone. *Mon. Wea. Rev.,* **124,** 849–874.

Stohl, A., 2001: A 1-year Lagrangian ''climatology'' of airstreams in the Northern Hemisphere troposphere and lowermost stratosphere. *J. Geophys. Res.,* **106,** 7263–7279.

——, and P. Seibert, 1998: Accuracy of trajectories as determined from the conservation of meteorological tracers. *Quart. J. Roy. Meteor. Soc.,* **124,** 1465–1484.

——, and T. Trickl, 1999: A textbook example of long-range transport: Simultaneous observation of ozone maxima of stratospheric and North American origin in the free troposphere over Europe. *J. Geophys. Res.,* **104,** 30 445–30 462.

——, G. Wotawa, P. Seibert, and H. Kromp-Kolb, 1995: Interpolation errors in wind fields as a function of spatial and temporal resolution and their impact on different types of kinematic trajectories. *J. Appl. Meteor.,* **34,** 2149–2165.

——, L. Haimberger, M. P. Scheele, and H. Wernli, 2001: An intercomparison of results from three trajectory models. *Meteor. Appl.,* **8,** 127–135.

——, S. Eckhardt, C. Forster, P. James, and N. Spichtinger, 2002: On the pathways and timescales of intercontinental air pollution transport. *J. Geophys. Res.,* **107**, 4684, doi:10.1029/2001JD001396.

——, and Coauthors, 2003: A backward modeling study of intercontinental pollution transport using aircraft measurements. *J. Geophys. Res.,* **108,** doi:10.1029/2002JD002862.

Susskind, J., P. Piraino, L. Rokke, L. Iredell, and A. Mehta, 1997: Characteristics of the TOVS pathfinder path A dataset. *Bull. Amer. Meteor. Soc.,* **78,** 1449–1472.

Trenberth, K. E., 1991: Storm tracks in the Southern Hemisphere. *J. Atmos. Sci.,* **48,** 2159–2178.

——, and J. M. Caron, 2000: The Southern Oscillation revisited: Sea level pressures, surface temperatures and precipitation. *J. Climate,* **13,** 4358–4364.

Vera, C., P. K. Vigliarolo, and E. H. Berbery, 2002: Cold season synoptic scale waves over subtropical South America. *Mon. Wea. Rev.,* **130,** 684–699.

Walker, G. T., and E. W. Bliss, 1932: World weather V. *Mem. Roy. Meteor. Soc.,* **4,** 53–84.

——, and ——, 1937: World weather VI. *Mem. Roy. Meteor. Soc.,* **4,** 119–139.

Wang, K.-Y., and D. E. Shallcross, 2000: A Lagrangian study of the three-dimensional transport of boundary-layer tracers in an idealised baroclinic-wave life-cycle. *J. Atmos. Chem.*, **35,** 227–247.

Webster, P. J., 1994: The role of hydrological processes in ocean–atmosphere interactions. *Rev. Geophys.*, **32,** 427–476.

Wernli, H., 1997: A Lagrangian-based analysis of extratropical cyclones, II, A detailed case study. *Quart. J. Roy. Meteor. Soc.*, **123,** 1677–1706.

——, and H. C. Davies, 1997: A Lagrangian-based analysis of extratropical cyclones, I, The method and some applications. *Quart. J. Roy. Meteor. Soc.*, **123,** 467–489.

——, and M. Bourqui, 2002: A Lagrangian ''1-year climatology'' of (deep) cross-tropopause exchange in the extratropical Northern Hemisphere. *J. Geophys. Res.*, **107**, 4021, doi:10.1029/2001JD000812.

World Meteorological Organization (WMO), 1957: Meteorology—A three dimensional science. *WMO Bull.*, **4,** 134–138.

Zhu, Y., and R. E. Newell, 1994: Atmospheric rivers and bombs. *Geophys. Res. Lett.*, **21,** 1999–2002.

Zierl, B., and V. Wirth, 1997: The influence of radiation on tropopause behaviour and stratosphere–troposphere exchange in an upper tropospheric anticyclone. *J. Geophys. Res.*, **102,** 23 883–23 894.